

JGR Earth Surface

RESEARCH ARTICLE

10.1029/2023JF007219

Key Points:

- We utilize a new generation of remote sensing data to study water movement beneath the vegetation canopy in salt marshes
- Small morphological features in marsh landscapes affect the spatial variability in water drainage within vegetated areas
- Salt marshes located at the same elevation within the local tidal range drain water differently

Supporting Information:

Supporting Information may be found in the online version of this article.

Correspondence to:

C. Donatelli,
dcarmine@bu.edu

Citation:






Donatelli, C., Passalacqua, P., Jensen, D., Oliver-Cabrera, T., Jones, C. E., & Fagherazzi, S. (2023). Spatial variability in salt marsh drainage controlled by small scale topography. *Journal of Geophysical Research: Earth Surface*, 128, e2023JF007219. <https://doi.org/10.1029/2023JF007219>

Received 19 APR 2023
Accepted 13 OCT 2023

Author Contributions:

Conceptualization: Carmine Donatelli, Paola Passalacqua, Sergio Fagherazzi
Data curation: Daniel Jensen, Talib Oliver-Cabrera, Cathleen E. Jones
Formal analysis: Carmine Donatelli
Funding acquisition: Paola Passalacqua, Sergio Fagherazzi
Methodology: Daniel Jensen, Talib Oliver-Cabrera, Cathleen E. Jones
Supervision: Paola Passalacqua, Sergio Fagherazzi
Writing – original draft: Carmine Donatelli
Writing – review & editing: Carmine Donatelli, Paola Passalacqua, Daniel Jensen, Talib Oliver-Cabrera, Cathleen E. Jones, Sergio Fagherazzi

Spatial Variability in Salt Marsh Drainage Controlled by Small Scale Topography

Carmine Donatelli^{1,2} , Paola Passalacqua¹ , Daniel Jensen³ , Talib Oliver-Cabrera³, Cathleen E. Jones³ , and Sergio Fagherazzi² 

¹Department of Civil, Architectural and Environmental Engineering, University of Texas at Austin, Austin, TX, USA, ²Department of Earth and Environment, Boston University, Boston, MA, USA, ³Jet Propulsion Laboratory, California Institute of Technology, Pasadena, CA, USA

Abstract Water movement in coastal wetlands is affected by spatial differences in topography and vegetation characteristics as well as by complex hydrological processes operating at different time scales. Traditionally, numerical models have been used to explore the hydrodynamics of these valuable ecosystems. However, we still do not know how well such models simulate water-level fluctuations beneath the vegetation canopy since we lack extensive field data to test the model results against observations. This study utilizes remotely sensed images of sub-canopy water-level change to understand how marshes drain water during falling tides. We employ rapid repeat interferometric observations from the NASA's Uninhabited Aerial Vehicle Synthetic Aperture Radar instrument to analyze the spatial variability in water-level change within a complex of marshes in Terrebonne Bay, Louisiana. We also used maps of herbaceous aboveground biomass derived from the Airborne Visible/Infrared Imaging Spectrometer-Next Generation to evaluate vegetation contribution to such variability. This study reveals that the distribution of water-level change under salt marsh canopies is strongly influenced by the presence of small geomorphic features (<10 m) in the marsh landscape (i.e., levees, tidal channels), whereas vegetation plays a minor role in retaining water on the platform. This new type of high-resolution remote sensing data offers the opportunity to study the feedback between hydrodynamics, topography and biology throughout wetlands at an unprecedented spatial resolution and test the capability of numerical models to reproduce such patterns. Our results are essential for predicting the vulnerability of these delicate environments to climate change.

Plain Language Summary Salt marshes are vegetated coastal ecosystems particularly susceptible to lateral erosion and sea-level rise. Hydrodynamic models are crucial to forecasting the vulnerability of these delicate environments to climate change, but we lack extensive field data to assess the accuracy of such models in vegetated flooded areas. Here, we utilize measurements collected from a NASA radar instrument flown on an airplane to determine how water moves beneath the vegetation canopy within a group of salt marshes located in the Mississippi River delta plain in Louisiana. Plant structure in the selected marshes was estimated from an imaging spectrometer which flew near-simultaneously with the radar instrument. Our study shows the utility of remotely sensed data to comprehend wetland hydrodynamics at a very high spatiotemporal resolution and improve the reliability of models that are needed to predict their fate.

1. Introduction

Salt marshes are vegetated landforms located at the boundary between land and sea. These valuable coastal ecosystems form in low-energy environments or near large rivers where fine sediments can accumulate (e.g., Fagherazzi et al., 2012). Salt marshes provide crucial ecosystem services to coastal communities since they act as buffers against storms, serve as nurseries for commercial fisheries, and sequester carbon (e.g., Leonardi et al., 2018). Their economic value has been estimated to be US\$5 million per square kilometer in the United States (Costanza et al., 2014, 2017).

Despite their ability to adapt in response to external disturbances, many studies document that salt marshes are disappearing at an alarming rate around the world due to lateral erosion and drowning (e.g., Carniello et al., 2011; Marani et al., 2011; Schuerch et al., 2018; Xu et al., 2022). Degradation of this precious habitat has a severe impact on coastal communities because it intensifies the risk of flooding and the impact of extreme events on cities and infrastructure (e.g., Temmerman et al., 2013; Orton et al., 2020).

Salt marshes expand or contract horizontally as a function of wind-waves and sediment availability, and they are potentially able to outpace the sea-level rise through inorganic matter accumulation and organic mass production (Marani et al., 2007, 2010). However, although organic matter allows vertical accumulation to offset the sea-level rise (Mudd et al., 2010), salt marshes cannot rely on this contribution alone. In fact, if mineral fluxes are not the primary driver in marsh accretion (i.e., the organic part exceeds the inorganic one), marsh structural fragility and edge failure may occur (Peteet et al., 2018).

Mariotti and Fagherazzi (2010) argue that the rate at which salt marshes erode for a given wave climate and sea-level rise rate ultimately depends on sediment supply. If the sediment input from rivers and the coastal ocean is low, salt marsh collapse can occur even without a sea-level rise. As such, the evaluation of sediment fluxes' direction and magnitude is fundamental to forecast the fate of salt marshes and determine their vulnerability to sea-level rise (e.g., Ganju et al., 2013, 2017). To make reliable estimations, it is crucial to precisely quantify the fluxes of water within these vegetated ecosystems and then focus on the fluxes of sediments.

Until now, numerical modeling has been the primary tool to investigate water and sediment movements in coastal wetlands (e.g., Beudin et al., 2017). However, numerical models of flooded vegetated areas may be unreliable, since we lack spatially distributed data to validate them. In fact, collecting field measurements beneath the vegetation canopy is challenging due to numerous practical limitations (e.g., Alsdorf et al., 2007).

Recently, remote sensing has been utilized to fill this data gap (e.g., Ayoub et al., 2018; Cathcart et al., 2020; Donatelli et al., 2023; Liao & Jiang, 2020; Wiberg et al., 2020). Airborne and spaceborne radars can perform multiple flights over the same region, allowing them to detect changes in sub-canopy water levels at a very high spatial resolution (5–10 m) (e.g., Oliver-Cabrera & Wdowinski, 2016). The Uninhabited Aerial Vehicle Synthetic Aperture Radar (UAVSAR) (Fore et al., 2015; Hensley et al., 2008) can perform rapid repeat interferometric surveys, offering a synoptic view of how water levels vary spatially with a revisit time of ~30 min (Oliver-Cabrera et al., 2021). For instance, interferometric products measured by UAVSAR have been used to calibrate water levels over extensive wetland areas (Wright et al., 2022).

In this paper, we employ UAVSAR water-level change products derived from data collected during Delta-X campaigns (Jones et al., 2022). Thus far, this data set has been mainly used to correct bathymetric information derived from lidar (e.g., Wright et al., 2022; Zhang, Jones, et al., 2022; Zhang, Wright, et al., 2022). Zhang, Jones, et al. (2022) and Zhang, Wright, et al. (2022) proposed an iterative/empirical methodology which corrects bed elevation in wetlands by using the difference between observed and modeled water-level change. They assumed that lowering (increasing) bed elevation allows for more (less) tidal propagation and therefore larger (smaller) water-level changes. However, as pointed out by the same authors, this approach, although it improves the accuracy of the model in reproducing changes in water level over time, can lead to unrealistic results for other hydrodynamic variables (e.g., flow velocities).

These UAVSAR observations open the possibility of studying wetland hydrodynamics at a spatial and temporal resolution that has not been possible with other remote sensing platforms. Our goal is to utilize high-spatial resolution, remotely sensed maps of water-level change beneath the vegetation canopy to determine the factors influencing water movement in marshes during a falling tide. This analysis is particularly important for quantifying the resilience of marshes (e.g., French & Spencer, 1993; Pannozzo et al., 2021; Sullivan et al., 2019). In fact, when water drains back to the ocean, nutrients and sediments are released within the surrounding environment, which has consequences for the long-term evolution of these vegetated ecosystems. Additionally, small creeks are typically ebb dominated because of the delay between water level and peak flow (Fagherazzi et al., 2008). As such, water drainage in marshes is critical for the evolution of the tidal network.

We used a complex of salt marshes located in Terrebonne Bay, Louisiana, as a test case. Here, we address the following hydrodynamic questions: (a) Are salt marshes characterized by the same elevation drain water differently? If so, what controls this difference? (b) What is the role of vegetation in retaining water over marsh surfaces? (c) Do small morphological features of the marsh landscape influence water-level change within the surrounding area? These questions are crucial to (a) understand water movement within these vegetated coastal habitats, and (b) determine the level of detail required for topographic data to accurately simulate marsh hydrodynamics via numerical modeling.

2. Study Site

Terrebonne Bay is a deltaic lagoon within the Mississippi Delta on the north coast of the Gulf of Mexico. Tides are diurnal with a mean astronomical tidal range of 0.32 m. The system is strongly event-driven (Reed, 1989).



Figure 1. Satellite image of Terrebonne Bay, Louisiana, USA. The rectangle highlights the location of the three selected salt marshes (here, we call this location “intensive site 0421”).

For instance, the effective tidal range reaches 0.7 m by combining astronomical and meteorological components (Mariotti, 2016). The bay presents a series of narrow and low-lying barrier islands (the Isles Dernieres and Timbalier chains) which separate the back-barrier basin from the Gulf of Mexico (Figure 1). The exchange of water between Terrebonne Bay and the coastal ocean occurs through tidal inlets, and it is affected mainly by tides and cold front passages (e.g., Reed, 1989). Sediments needed for marsh accretion are derived from erosional processes occurring within the bay (e.g., bed erosion, marsh lateral erosion), and are delivered from offshore into the lagoon by storms (Cortese & Fagherazzi, 2022). The lagoon is located between the Mississippi River Delta and the Atchafalaya Delta (Figure 1). The presence of these two systems creates differences in vertical stratification of the water column between the eastern and western parts of the bay. Such differences influence biological processes within Terrebonne Bay and are highly variable due to seasonal changes in wind conditions (Hetland & DiMarco, 2008).

3. Methods

We utilize remotely sensed maps of sub-canopy water-level change to analyze drainage patterns over three marshes in Terrebonne Bay, Louisiana, USA. UAVSAR images were collected in two distinct temporal windows: 12 April 2021 between 19:29 and 22:59 (UTC time), and 4 September 2021 between 16:21 and 20:08 (UTC time). Hydrodynamic conditions are similar during the two campaigns, but vegetation characteristics present marked differences. As such, we can unravel the effect of vegetation on water-level change (WLC) by comparing UAVSAR data measured in the two selected temporal windows.

WLC on marsh platforms is affected by water conveyance. The latter can be expressed by the empirical Manning's formula that applies to uniform flow in open channels:

$$q = \frac{1}{n} \cdot h^{5/3} \cdot i^{1/2} \quad (1)$$

where n is the Manning's roughness coefficient, h is the water depth, and i represents the water-surface slope. In numerical models, the simplest way to account for the effect of vegetation on a depth-averaged flow is to increase the roughness coefficient with respect to unvegetated areas (e.g., Beudin et al., 2016). Similarly, model calibration in channels and open water is often performed by varying the roughness coefficient until the simulated water levels match those measured in the field (e.g., Cortese et al., 2023).

To determine the influence of water depth and friction on WLC, we make use of (a) high-spatial resolution topographic data (Figure 2a) (Christensen et al., 2023); and (b) two high-spatial resolution maps of herbaceous aboveground biomass (AGB) obtained using AVIRIS-NG hyperspectral imager (see Figure 2b for the AGB distribution during spring) (Jensen et al., 2022). Note that we employ two AGB maps because the UAVSAR

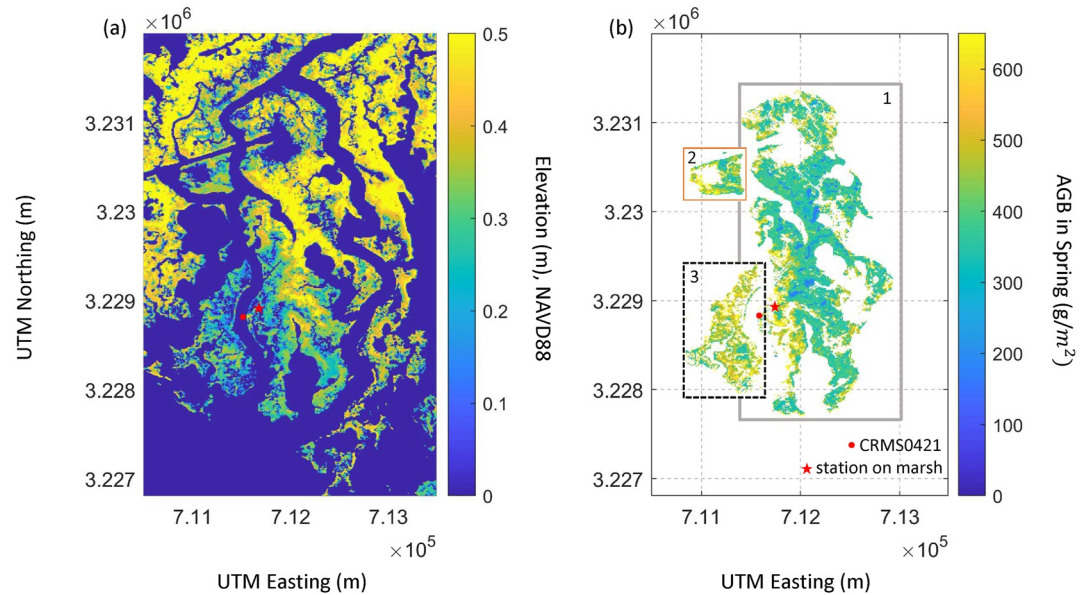


Figure 2. (a) Topography of the study site. Topographic data are reported with respect to NAVD88. (b) Above ground biomass (AGB) in spring. The (orange) thin lines and the (black) dashed lines highlight marshes 2 and 3, respectively, while the remaining area represents marsh 1 (this area is highlighted by the thicker lines). The dot shows the location of the CRMS0421 station, and the star indicates the location over the marsh platform where field observations of water levels were collected.

campaigns occurred in two different seasons (i.e., spring and fall, see how vegetation structure changes with seasons in Table 1 (Castañeda & Solohin, 2021)). The intensive site was dominated by *Spartina alterniflora* during the spring campaign, and by a mix of *Spartina alterniflora* and *Juncus roemerianus* during the March–April campaign (Figure 3).

It is important to highlight that part of the measurements collected during the 4 September 2021 UAVSAR flight is affected by atmospheric effects (see Figure S1 in Supporting Information S1 and Movie S1), which prevents the use of these data. This means that we cannot use all the data taken in this campaign. More specifically, WLC measured over the largest marsh (marsh 1 in Figure 2b) is partially corrupted due to variations in atmospheric properties between the different SAR acquisitions (e.g., Hanssen, 2001).

The procedure adopted here to analyze the spatial variability in salt marsh drainage can be summarized as follows: (a) we use UAVSAR data (Section 3.1) and field observations of water level (Section 3.2) to evaluate whether UAVSAR provides reliable estimations of WLC on marsh surfaces; (b) we employ the WLC measurements collected during the 12 April 2021, UAVSAR flight to determine whether marshes characterized by the same elevation present comparable changes in water level within the same temporal window; (c) we utilize the AGB map in spring (Section 3.3, see Figure 2b) to evaluate the effect of spatial variations in vegetation characteristics on the distribution of WLC; (d) we use UAVSAR data to understand the role of small features in the marsh landscape (i.e., levees and channels) on water movement; (e) we employ WLC measurements collected during the 12

Table 1
Mean Height, Mean Stem Diameter, and Stem Density (Latitude 29.1714, Longitude 90.8223)

| | | Height (cm) | Diameter (cm) | Density (stems/m ²) |
|--|-----|-------------|---------------|---------------------------------|
| Supratidal <i>S. alterniflora</i> (spring) | AGB | 48.71 | 4.52 | 112 |
| Supratidal <i>S. alterniflora</i> (spring) | AGN | 46.62 | 6.03 | 128 |
| Supratidal <i>S. alterniflora</i> (fall) | AGB | 72.4 | 6.5 | 304 |
| Supratidal <i>S. alterniflora</i> (fall) | AGN | 44.3 | 6.17 | 48 |

Note. The data were collected between 2021-03-21 and 2021-03-31 during the Delta-X Spring 2021 deployment, and between 2021-08-19 and 2021-08-27 during the Fall deployment.

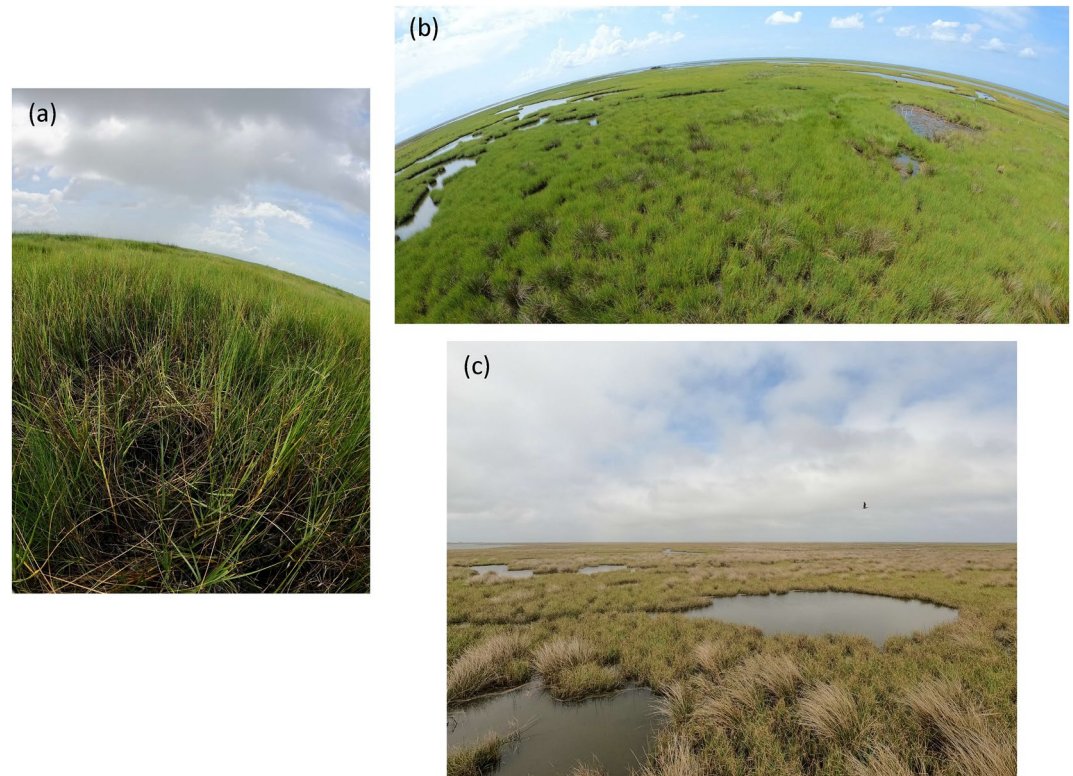


Figure 3. Field images of vegetation types in the (a, b) spring and (c) fall campaigns.

April 2021, and the 4 September 2021, UAVSAR flights to determine the influence of seasonal changes in AGB on WLC over marshes 2 and 3 (i.e., where UAVSAR data are not affected by atmospheric effects during the 4 September 2021, UAVSAR flight, see Figure 2b).

3.1. UAVSAR Interferometry

UAVSAR is a synthetic aperture imaging radar deployed on a Gulfstream-3 aircraft that collects measurements of Earth's surface change from 12.5 km altitude. The instrument is a fully polarimetric (i.e., it transmits horizontal and vertical pulses and receives returns from each in both polarizations), left-looking synthetic aperture radar that operates in L-band ($\lambda = 0.2379$ m of wavelength) with center frequency of 1.2575 GHz and 80 MHz of bandwidth. The radar images a region 22 km wide, with an incidence angle ranging between $\sim 22^\circ$ (near range) to $\sim 67^\circ$ (far range) (Garcia-Pineda et al., 2013).

A collection of UAVSAR measurements were performed over the entire salt-marsh system in Terrebonne Bay. The region was scanned six times between 19:29 and 22:58 (UTC time) on 12 April 2021, and between 16:21 and 20:08 (UTC time) on 4 September 2021. The goal of these measurements is to take advantage of the rapid-repeat pass capability of UAVSAR and capture WLC over flooded surfaces with emergent vegetation. This capability is possible due to the double-bounce radar-pulse return that bounces from both the water surface and the vegetation (Daboor & Brisco, 2018; Lu & Kwoun, 2008), allowing the measurement of WLC in areas with sparse gauge coverage. In particular, we used pairs of rapid-repeat pass SAR acquisitions acquired by UAVSAR to form sets of interferograms employing the InSAR Scientific Computing Environment (Rosen et al., 2000). We then performed a phase unwrapping to quantify the number of 2π cycles, to be able to accurately derive the total displacement in water level. Once the interferograms were unwrapped, we used them to estimate the InSAR-derived WLC time series, as described in the product documentation available at the ORNL DAAC (https://daac.ornl.gov/DELTA/guides/DeltaX_L3_UAVSAR_WaterLevels.html) (Jones et al., 2022). This method can be similarly applied to different wetland types (e.g., mangroves). However, its effectivity will be highly dependent on the repeat pass schedule of the observing sensor as well as the type of vegetation observed. If the vegetation has a soft stem, its

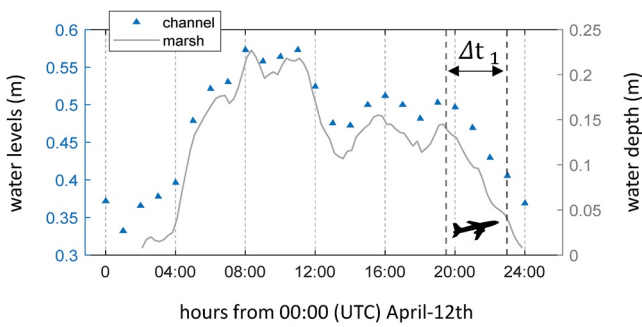


Figure 4. Field measurements of water levels (m) in the channel (triangles, CRMS-421 station, see Figure 2), and water depth over marsh (solid line, lat 29.170201, lon -90.823649 , see Figure 2). Water levels are measured with respect to NAVD88. These observations were collected in 12 April 2021. Δt_1 represents the interval of time in which the Uninhabited Aerial Vehicle Synthetic Aperture Radar flight took place.

scattering properties will change rapidly and data acquisition will require a very short repeat observation time, whereas woody vegetation may allow for a longer temporal baseline in the SAR acquisition pattern (Oliver-Cabrera et al., 2021). Note that the method cannot be applied to submerged vegetation, for example, seagrass.

3.2. Field Measurements of Water Levels

The Coastwide Reference Monitoring System (CRMS) was designed by the Louisiana State Wetlands Authority, and the Coastal Wetlands Planning, Protection, and Restoration Act Task Force to evaluate the effectiveness of restoration projects at multiple spatial scales along the Louisiana coastline. Instruments at nearly 400 sites have continually monitored soils, hydrology, land change, and vegetation since 2003. These stations provide hourly water-level data, which are used to analyze spatial variations in hydrodynamic conditions at different temporal scales. We employ water-level observations from the CRMS-0421 station (see red dot in Figure 2b) to evaluate how water levels vary in a channel adjacent to the three selected marshes during the UAVSAR flights.

These data are complemented with field measurements of water levels on the neighboring marsh platform (see red star in Figure 2b). The instrument on the marsh was installed at approximately 3 cm above the soil surface (thus we do not have data when water level was lower than 3 cm) and collected water-level data every 20 min. Measurements are expressed with respect to NAVD88.

3.3. Above Ground Biomass (AGB)

We utilize two maps of herbaceous aboveground biomass (AGB), derived from Airborne Visible Infrared Imaging Spectrometer-Next Generation (AVIRIS-NG) data, developed by Jensen et al. (2022), D. Jensen et al. (2023), and D. J. Jensen et al. (2023) for the spring and fall seasons. AVIRIS-NG is an imaging spectrometer that measures radiance at 5 nm sampling across 425 bands in the Visible to Short-Wave Infrared (VSWIR) spectral range (380–2,500 nm). The L1 radiance data were processed to L2 surface reflectance products with atmospheric correction (Thompson et al., 2019), with further corrections applied to adjust for Bidirectional Reflectance Distribution Function effects (Greenberg et al., 2022; Thompson et al., 2022). AGB, quantified as dry biomass in grams per square meter (g/m^2), was estimated from the BRDF-adjusted surface reflectance and a coincident AGB field survey (Castañeda-Moya & Solohin, 2022). A machine learning model was generated to estimate AGB by comparing local pixel reflectance spectra with coincident in situ samples of herbaceous vegetation AGB. This model ($R^2 = 0.89$, Mean Absolute Error = $109.30 \text{ g}/\text{m}^2$) was then scaled to the AVIRIS-NG mosaic imagery to map herbaceous AGB across the Terrebonne Basin. The instrument is also used to measure water quality and suspended sediment concentration in coastal regions (e.g., Jensen et al., 2019). The map has a spatial resolution of $\sim 5 \text{ m}$. The AGB map is depicted in Figure 2b. A detailed description of how the AGB map was obtained is reported in Jensen et al. (2022).

4. Results

Field measurements of water levels show that the tidal signals in the channel and over the marsh are generally in phase (Figure 4). However, a small phase shift between these two signals may exist and be spatially variable, and it depends on the distance between the channel and the location where water levels are measured over the marsh. We use data from UAVSAR to analyze the spatial variability in WLC over the selected marshes (Figure 2b). The maps representing WLC on marsh platforms are shown in Figure S2 in Supporting Information S1 for the 12 April 2021, UAVSAR flight (see Supporting Information S1); the temporal window (Δt_1) in which the UAVSAR campaign took place is shown in Figure 4. UAVSAR-derived WLC in the marsh pixels located next to the CRMS station 0421 matches well the field measurements.

Since WLC on marsh platforms depends on flow conveyance, we plot UAVSAR-derived WLC as a function of marsh elevation (see Section 4.1) and AGB (see Section 4.2). Then, we select various marsh sub-regions and focus

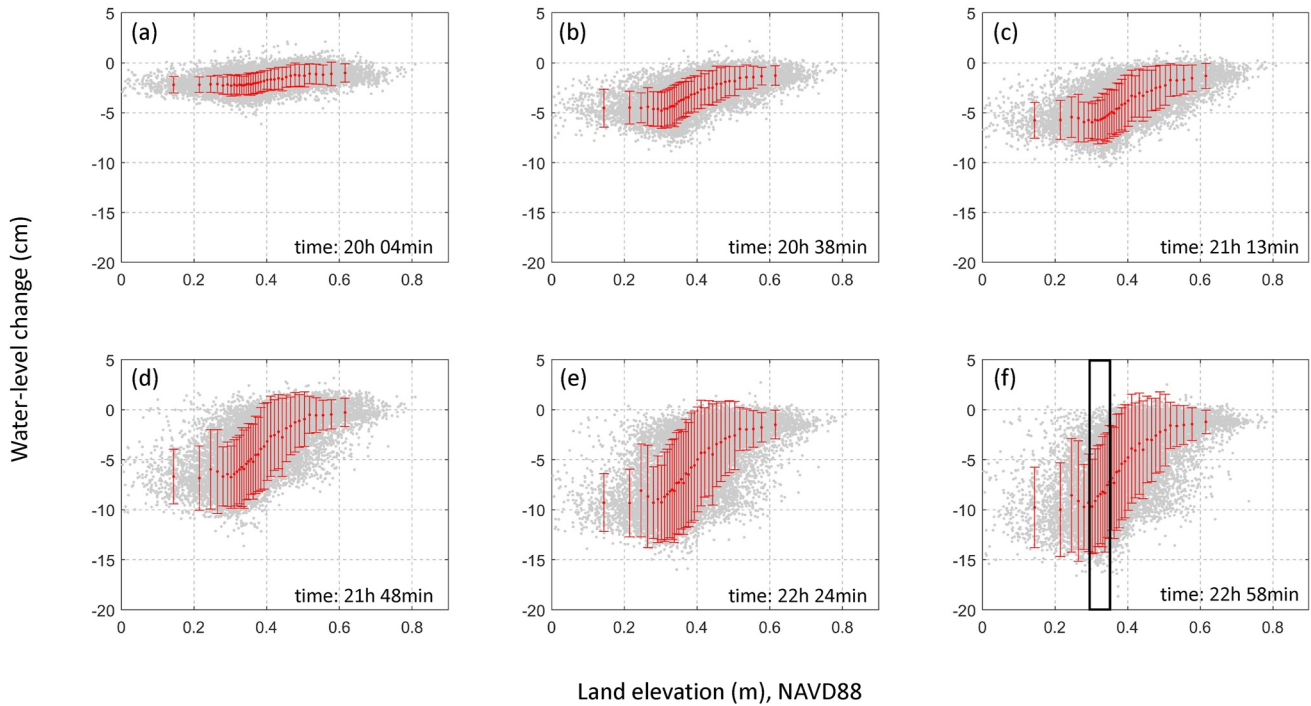


Figure 5. UAVSAR-derived WLC (cm) as a function of marsh elevation (m) for different intervals of time, starting at $t = 19:29$ UTC and ending at the time indicated on each plot. Red dots represent median values and the red bars indicate the interquartile range. WLC was measured during the 12 April 2021 Uninhabited Aerial Vehicle Synthetic Aperture Radar flight. The rectangle in (f) shows the interval of marsh elevation that is considered in Figure 6.

on the presence of small geomorphic features (width smaller than 10 m) in the marsh landscape. Such geomorphic features may affect water transport in marshes, and consequently WLC on platforms (see Section 4.3). In the same subsection, we also evaluate the effect of seasonal changes in vegetation characteristics on WLC.

4.1. WLC as a Function of Marsh Elevation

We plot WLC estimated during the 12 April 2021 UAVSAR flight as a function of marsh height (Figure 5). The values are changes in water level relative to the first acquisition, which was made at 19:29 UTC. Our aim is

to determine if vegetated pixels (hereinafter called also marsh pixels) characterized by the same elevation within the local tidal range experience a similar change in water level over the selected temporal window (Figure 5). We modified the spatial resolution of the UAVSAR data (and later that of AVIRIS-NG, see Section 4.2) to obtain the same resolution of the available bathymetry (i.e., 10 m). In particular, we resampled the raster to a lower resolution by using a standard method for resampling (i.e., nearest neighbor). Figure 5 depicts WLC as a function of marsh height in six different temporal windows (these six temporal windows start at 19:29, and end at 20:04, 20:38, 21:13, 21:48, 22:24 and 22:58 respectively). Note that WLC increases in absolute value with respect to the first UAVSAR acquisition. Interestingly, vegetated pixels with a similar elevation can exhibit a different change in water level, indicating that water can drain differently from locations of similar elevation, depending on their location within the marsh. This result is highlighted by the interquartile range in UAVSAR-derived WLC, which varies as a function of marsh elevation (Figure 5).

The substantial variability in WLC shown by marsh pixels located at the same elevation is potentially related to spatial variations in vegetation

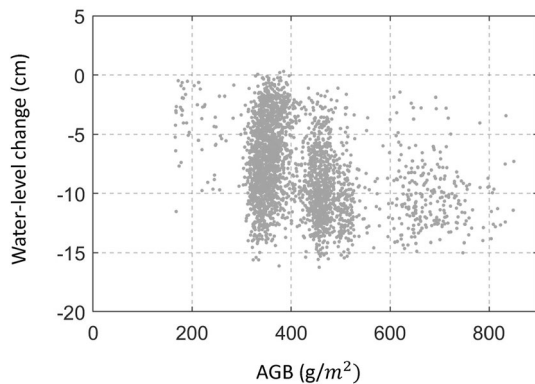


Figure 6. UAVSAR-derived WLC (cm) as a function of AGB (g/m^2). WLC was measured during the 12 April 2021 Uninhabited Aerial Vehicle Synthetic Aperture Radar flight during the time interval 19:29–22:58 UTC. We only consider marsh pixels with an elevation between 0.3 and 0.35 m (see rectangle in Figure 5f).

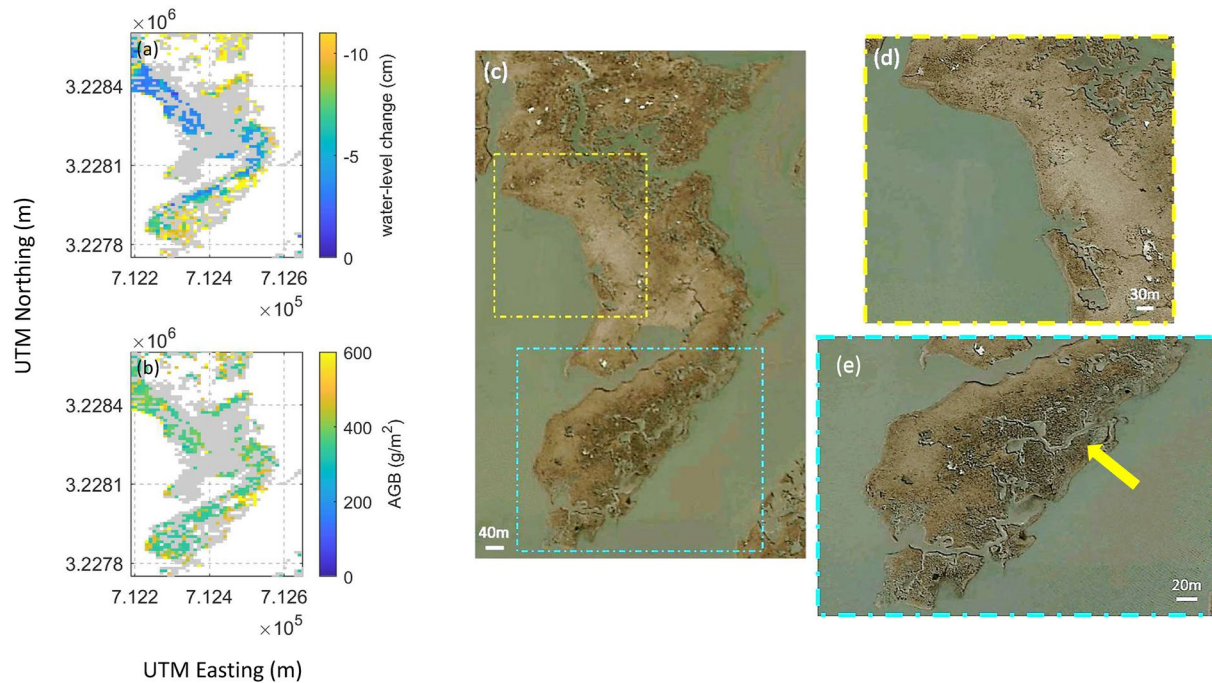


Figure 7. Spatial distribution of (a) UAVSAR-derived WLC (cm), and (b) AGB (g/m^2) values in spring for a sub-region of marsh 1. WLC was measured during the 12 April 2021 Uninhabited Aerial Vehicle Synthetic Aperture Radar flight. Satellite images: (c) entire sub-region; (d, e) close up of two different parts of the selected sub-region (i.e., area without channels and highly channelized area). The arrow indicates the presence of small tidal channels with widths of 2 and 5 m (image ©Google, Landsat/Copernicus).

characteristics. We investigate the relationship between changes in water level and above ground biomass in the next subsection.

4.2. Effect of Vegetation on the Distribution of WLC

We utilize the map of AGB in the spring (Figure 2b) to determine the effect of vegetation on WLC during the 12 April 2021 UAVSAR flight. We only consider marsh pixels with an elevation between 0.3 and 0.35 m (since the majority of vegetated pixels in the selected group of marshes have an elevation within this range). In other words, we fixed the marsh height (see rectangle in Figure 5f) to evaluate the relationship between WLC and AGB. When WLC is plotted as a function of the above ground biomass (Figure 6), the results reveal a weak correlation between these two variables. Surprisingly, changes in water level (in absolute value) within the selected temporal window of 3.5 hr seem to increase with greater values of above ground biomass.

It should be noted that WLC measured by UAVSAR occurs only in the portion of the water column occupied by plants. This can be easily verified by comparing field measurements of water level over the marsh (Figure 4) with the data of vegetation structure collected between 21 March 2021 and 31 March 2021 (Table 1). The maximum water level observed over the marsh during the selected temporal window is 15 cm, which is indeed smaller than the plant height reported in Table 1.

4.3. Effect of Small Geomorphic Features in Marsh Landscape on WLC

We analyze images from satellite (Google Earth) to identify the presence of small geomorphic features in the marsh landscape. Such elements may affect water conveyance on marsh platforms, allowing for approximately tidal propagation within surrounding areas. First, we map the spatial distribution of WLC and AGB within the selected sub-regions. Then, we utilize images from satellite to understand why pixels with similar elevation drain water differently.

We start by considering the sub-region depicted in Figure 7 (this sub-region is part of marsh 1 depicted in Figure 2b). Here, we show the spatial distribution of (a) WLC measured during the 12 April 2021 UAVSAR

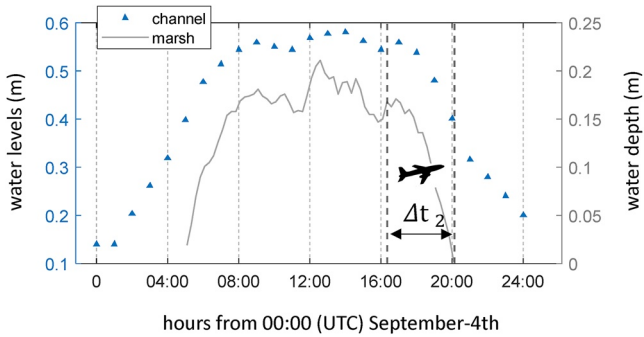


Figure 8. Field measurements of water levels (m) (i) in the channel (CRMS-421 station), and (ii) over the marsh (lat 29.170201, lon -90.823649). Water levels are measured with respect to NAVD88. These observations were collected in 4 September 2021. Δt_2 represents the interval of time in which the Uninhabited Aerial Vehicle Synthetic Aperture Radar flight took place.

campaign (Figure 7a), and (b) AGB values during the spring (Figure 7b). We focus only on pixels with an elevation between 0.3 and 0.35 m. These pixels present substantial variability in WLC with values ranging between 0 and 11 cm (Figure 7a).

We show images of this sub-region in Figures 7c–7e. These images reveal that the vegetated pixels exhibiting larger values of WLC are located next to tidal channels, which are not captured by the available bathymetric data (see the arrow in Figure 7e). Such channels (width ranging between 1 m and 10 m) help drain water from the marsh surface, therefore increasing WLC within the adjacent vegetated pixels (see Figure 7e).

We apply the same approach to marshes 2 and 3 (see Figure 2b). UAVSAR data from another campaign are also available for these marshes. Figure 8 shows water levels measured at the CRMS-0421 station in the channel and over the marsh for 4 September 2021. In the same figure, we show the temporal window in which the UAVSAR flight took place (Δt_2).

Histograms of WLC and AGB are reported in Figure 9. Table 2 lists the mean, median, standard deviation, interquartile range, and skewness for each distribution. Here, we use the median as a measure of the typical value of WLC. Note that the typical value is greater for the 4 September 2021 UAVSAR campaign compared to the 12 April 2021 UAVSAR campaign. This result is consistent with field observations of water level collected over the marsh (Figures 4–8).

Spatial distributions of WLC and AGB for marsh 2 are shown in Figure 10. We only consider pixels with an elevation between 0.35 and 0.40 m (since the majority of pixels in marsh 2 have an elevation within this range). WLC (Figures 10a and 10b) within the two selected temporal windows presents a similar spatial distribution ($R = 0.64$). In contrast, the AGB maps do not exhibit a similar spatial pattern between spring and fall ($R = -0.22$). This result implies that, despite both the substantial increase in AGB values (see histograms in Figures 9c and 9d) and the occurrence of marked changes in their spatial distribution, WLC remains fairly similar within the two UAVSAR campaigns. By using satellite images (Figures 10e–10g), we observe that the area of the marsh experiencing greater changes in water level (Figures 10a and 10b) is fragmented (see Figures 10f and 10g; the large arrows in Figure 10g highlight the presence of two small tidal channels). In contrast, the WLC is lower where tidal channels are absent (see for instance the marsh area highlighted by the small arrow in Figure 10g).

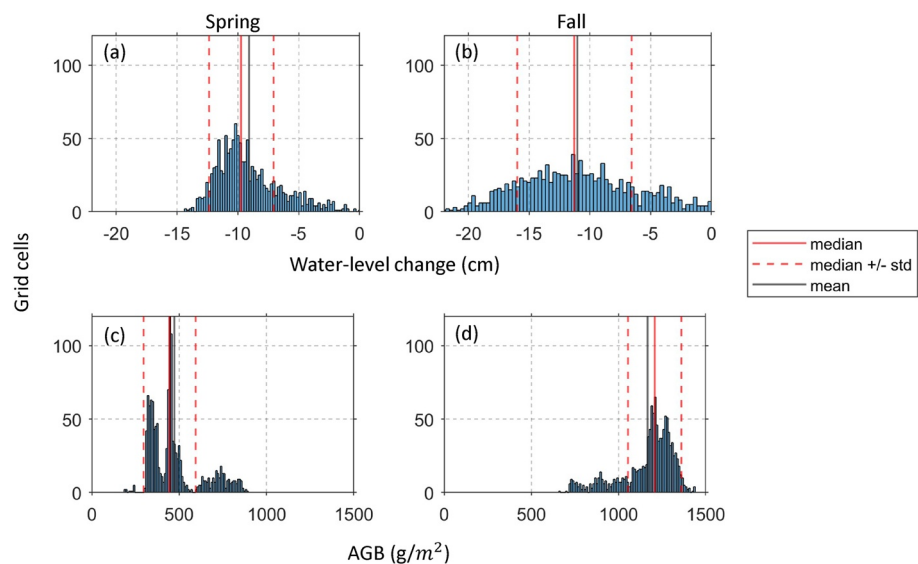


Figure 9. Histograms of (a, b) WLC and (c, d) AGB for marsh 2 (see Figure 2b) during (a, c) the 12 April 2021 and (b, d) 4 September 2021 Uninhabited Aerial Vehicle Synthetic Aperture Radar flights. The solid red line represents the median value, while the dashed lines represent the median value plus/minus one standard deviation. The black line represents the mean value. WLC is considered positive if it corresponds to an increase in water level in the selected temporal window.

Table 2
Mean, Median, Standard Deviation, Interquartile Range, and Skewness of WLC (cm) and AGB (g/cm²) on Marsh 2 (See Figure 2b)

| | Median | Mean | Standard deviation | Interquartile range | Skewness |
|-------------------------------------|--------|--------|--------------------|---------------------|----------|
| Water-level change (cm), campaign 1 | −9.73 | −9.08 | 2.68 | 3.32 | 0.91 |
| AGB (g/cm ²), spring | 445 | 473 | 148 | 145 | 1.10 |
| Water-level change (cm), campaign 2 | −11.28 | −11.05 | 4.69 | 6.61 | 0.18 |
| AGB (g/cm ²), fall | 1,208 | 1,168 | 154 | 159 | −1.20 |

Finally, we focus on the third marsh. Histograms of WLC and AGB highlight differences between the two selected temporal windows (Figure 11). Table 3 shows the mean, median, standard deviation, interquartile range, and skewness for each distribution. We plotted maps of WLC and AGB in spring and fall (Figure 12). Note that a low correlation exists between the two maps of WLC ($R = 0.33$) and between the maps of AGB ($R = -0.21$). By comparing Figures 12a and 12b with satellite images (Figure 13), we observe that levees are present where WLC is much lower compared to the median value (see for instance the arrow in Figure 13b). Furthermore, we note that this marsh is highly fragmented (Figure 13c), and, as such, exhibits a smaller standard deviation of WLC compared to marsh 2 (see Tables 2 and 3).

5. Discussion

We utilized a new generation of remotely sensed data to study the interactions of vegetation, topography, and flow on marsh platforms. These interactions have been explored for three salt marshes located in Terrebonne Bay, Louisiana (see Figures 1 and 2). In particular, we focused on unraveling what factors influence spatial variations in WLC on marsh platforms at hourly time scales. To this end, we used (a) multiple images of UAVSAR-derived WLC collected during falling tides, (b) bathymetric data from lidar, and (c) high-spatial resolution maps of AGB obtained through AVIRIS-NG.

5.1. WLC as a Function of Marsh Topography

Our results reveal that marsh platforms exhibit substantial spatial variability in WLC (e.g., Figure 5). Interestingly, marsh pixels characterized by the same elevation within the local tidal range present marked differences in WLC. Part of this variability can be explained by the presence of errors in the lidar data. In particular, the laser cannot penetrate into thick vegetation canopies leading to a positive bias in bed elevation. Such bias is spatially variable and depends on vegetation density (e.g., Cooper et al., 2019; Medeiros et al., 2015; Rogers et al., 2018). This result means that we cannot correct topographic errors by uniformly lowering the bathymetry, but an ad hoc change in bed elevation is needed for each point of the domain.

Zhang, Jones, et al. (2022) and Zhang, Wright, et al. (2022) proposed to correct wetland bathymetry (i.e., remove the positive bias) by employing data from UAVSAR and numerical modeling. However, it turned out in their study that the derived topographic corrections were either positive or negative (i.e., bed elevations were also biased toward a lower elevation). Since the bias in bathymetric information due to the laser's inability to penetrate vegetation can be only positive, it is likely that the negative bias can be related to the presence of geomorphic elements in the marsh that are not captured in the model grid (e.g., Blanton et al., 2010). These topographic features (e.g., small levees) promote water retention within the surrounding vegetated areas, leading to a smaller WLC.

It is worth noting that the empirical/iterative approach of Zhang, Jones, et al. (2022) and Zhang, Wright, et al. (2022) could modify bed elevations even in regions where corrections are not needed. If the spatial resolution of the model is too coarse to capture the presence of small tidal creeks (note that tidal creeks facilitate water drainage on marsh surface and therefore increase WLC), a decrease in bed elevation and/or friction would be required. Specifically, these modifications would increase water conveyance on platforms, and consequently augment the change in water level within the selected temporal window. On the other hand, corrections in bathymetry and/or friction would not only alter local hydrodynamics (i.e., where changes are made) but also propagate to areas downstream leading to an overall decrease in model accuracy in reproducing WLC within vegetated areas. As such, it is essential that topographic data have sufficient spatial resolution to identify small tidal creeks and levees on marsh platforms, for example, 1-m spatial resolution. This condition is important to

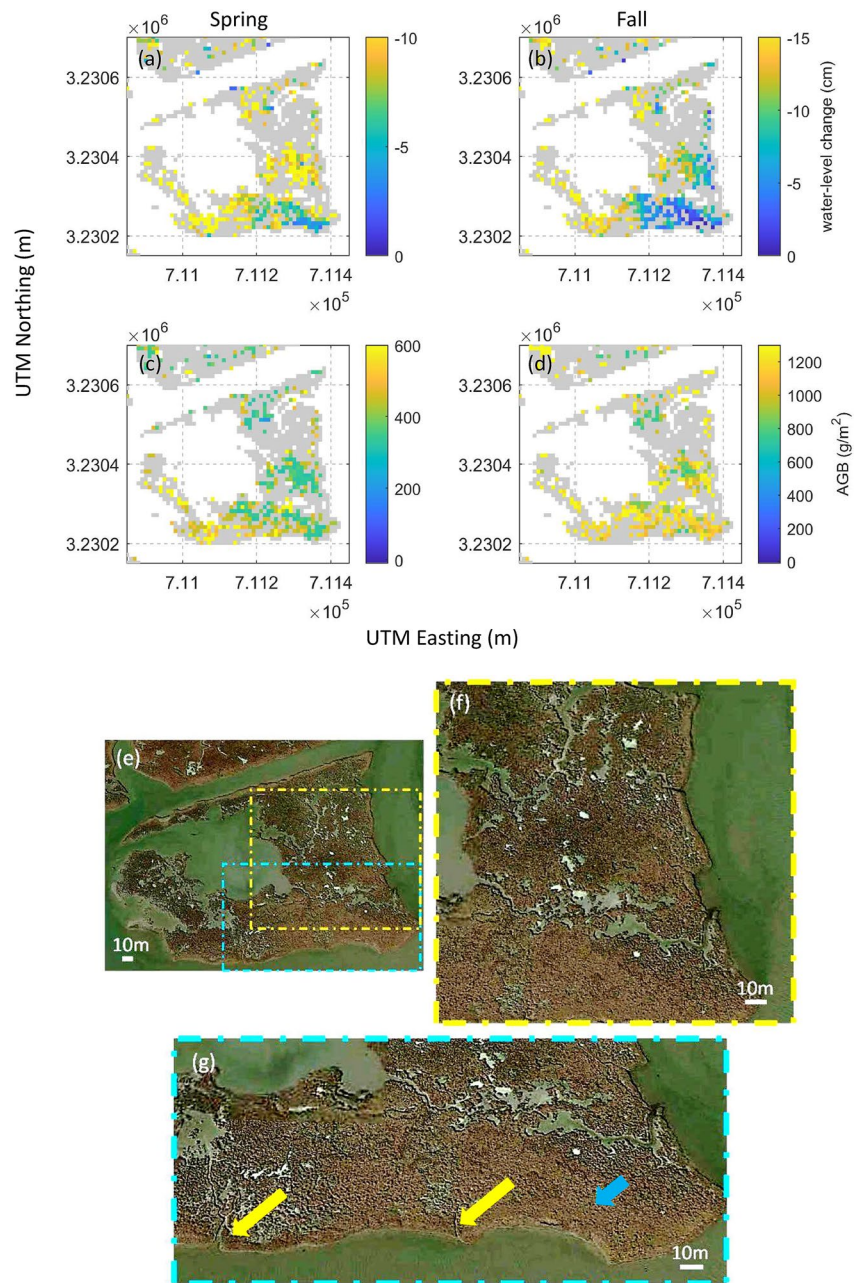


Figure 10. Spatial distribution of (a, b) UAVSAR-derived WLC (cm), and (c, d) AGB (g/m^2) values in spring (a, c) and fall (b, d) for marsh 2. WLC was measured during the 12 April 2021 and 4 September 2021 Uninhabited Aerial Vehicle Synthetic Aperture Radar flights. Satellite images: (e) entire marsh 2; (f, g) close up of two different parts of the selected marsh. Images (f, g) highlight the presence of small tidal channels in the marsh landscape. The large (yellow) arrows highlight the presence of two small tidal channels with a width of 2–3 m. The small (blue) arrow indicates an area of the marsh where tidal channels are absent (image ©Google, Landsat/Copernicus).

(a) capture the enormous spatial variability in hydrodynamic conditions across marsh landscapes via numerical modeling; (b) minimize possible fictitious changes in bed elevation and/or friction introduced using the procedure proposed by Zhang, Jones, et al. (2022) and Zhang, Wright, et al. (2022); and (c) remove the effects related to errors in topography.

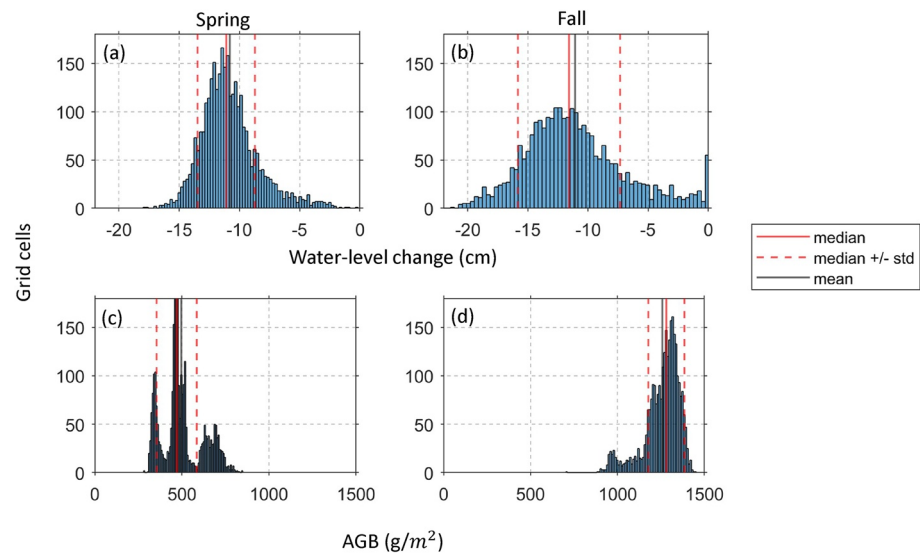


Figure 11. Histograms of (a, b) WLC and (c, d) AGB for marsh 3 (see Figure 2b) during (a, c) the 12 April 2021 and (b, d) 4 September 2021 Uninhabited Aerial Vehicle Synthetic Aperture Radar flights. The solid red line represents the median value, while the dashed lines represent the median value plus/minus one standard deviation. The black line represents the mean value. WLC is considered positive if it corresponds to an increase in water level in the selected temporal window.

5.2. Effect of Vegetation on WLC

The interaction between flow and vegetation is complex and has been explored at different spatial and temporal scales (e.g., Donatelli et al., 2019; Mazda et al., 1997; Temmerman et al., 2005; Wu et al., 2001). Until now, we did not have observations that provide a spatially continuous view of how tides propagate in wetlands. UAVSAR repeat-pass interferometry provides, for the first time, a synoptic view of WLC across vegetated areas. This remote sensing technique allows us to study the hydrodynamics in these ecosystems at an unprecedented spatial resolution.

Water retention on marsh platforms depends on (a) the degree of channelization, which affects the transport of water from the marsh interior toward the surrounding environment; (b) levees, which obstruct the flow and do not allow the water to drain following the shortest and steepest path, and (c) vegetation, which exerts a drag on the flow and thus slows down tidal currents. In this study, we show that WLC on marshes during falling tides is not affected by spatial and temporal changes in AGB (e.g., Figure 6). This finding is a counterintuitive one since it is well known that vegetation increases friction on tidal currents (e.g., Gerkema, 2019) and alters spatial flow patterns in tidal landscapes (e.g., Temmerman et al., 2007, 2013). However, we argue that in highly channelized marshes, such as those in Terrebonne Bay, the ebb flow is preferentially transported via channels. Therefore, vegetation has a limited effect in retaining water on marsh surfaces. This result is broadly consistent with Montgomery et al. (2018) and Pelckmans et al. (2023), who found a similar behavior in mangroves. They both showed that vegetation attenuates long waves only if the transport of water through the vegetation is the main mechanism of fluid transport. If creek flow dominates, the density of mangrove vegetation has a minimal effect on the attenuation of water levels (e.g., Horstman et al., 2015). Our finding also agrees with Zhang, Jones,

Table 3
Mean, Median, Standard Deviation, Interquartile Range and Skewness of WLC (cm) and AGB (g/cm²) on Marsh 3 (See Figure 2b)

| | Median | Mean | Standard deviation | Interquartile range | Skewness |
|-------------------------------------|--------|--------|--------------------|---------------------|----------|
| Water-level change (cm), campaign 1 | -11.10 | -10.79 | 2.38 | 2.66 | 0.88 |
| AGB (g/cm ²), spring | 471 | 497 | 114 | 83 | 0.61 |
| Water-level change (cm), campaign 2 | -11.58 | -11.08 | 4.25 | 5.14 | 0.56 |
| AGB (g/cm ²), fall | 1,281 | 1,257 | 103 | 117 | -1.28 |

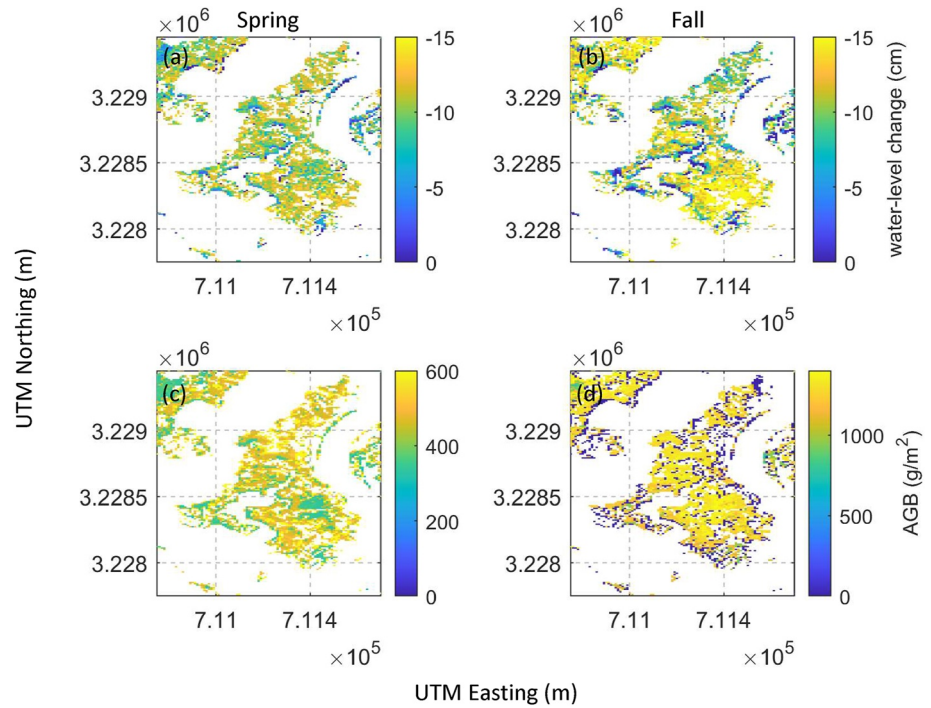


Figure 12. Spatial distribution of (a, b) UAVSAR-derived WLC (cm), and (c, d) AGB (g/m^2) values in spring (a, c) and fall (b, d) for marsh 3. WLC was measured during the 12 April 2021 and 4 September 2021 Uninhabited Aerial Vehicle Synthetic Aperture Radar flights.

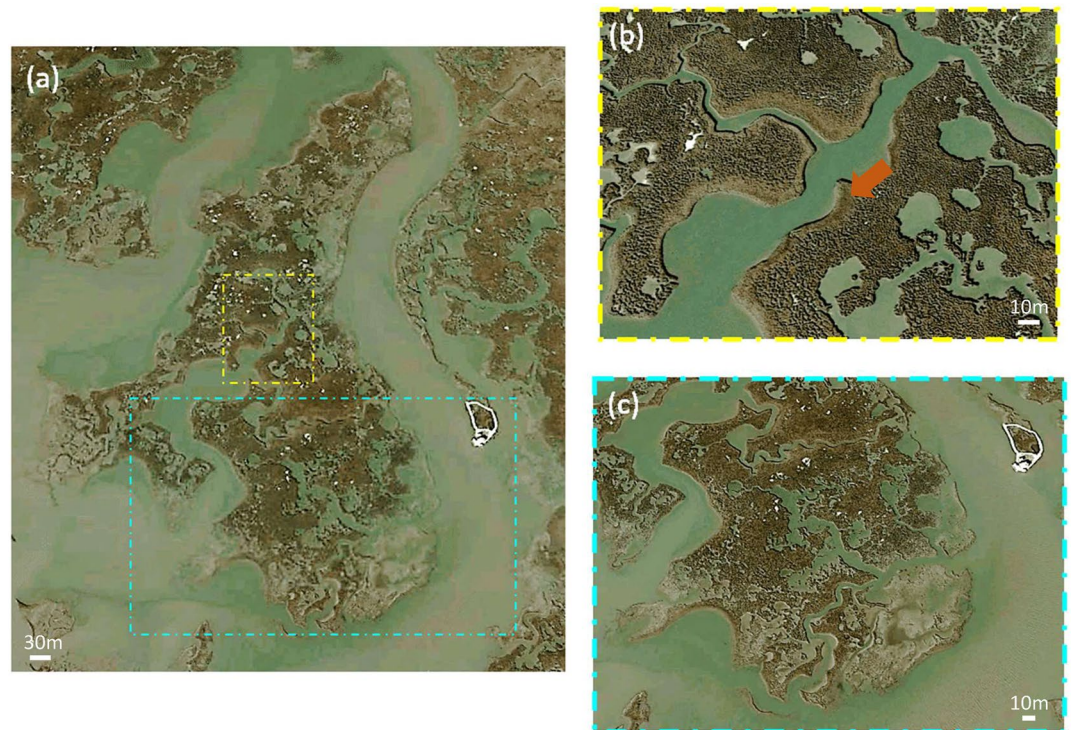


Figure 13. Satellite images: (a) entire marsh 3; (b, c) close up of two different parts of the selected marsh. Image (b) highlights the presence of levees, whereas image (c) shows a sub-region of marsh 3, which is highly channelized. The arrow indicates the presence of levees (image ©Google, Landsat/Copernicus).

et al. (2022), who showed through numerical modeling that large variations in friction on marsh platforms have a minimal impact on WLC.

Another factor that could diminish the effect of vegetation on WLC is water depth. When vegetation is fully submerged and occupies only part of the water column, large-scale sheet flow (i.e., flow above the canopy) becomes important and relative spatial differences in friction decrease (Fagherazzi et al., 2012; Nepf, 2012; Temmerman et al., 2005). The two 3.5-hr UAVSAR campaigns were conducted during falling tides with an initial water level in the channel of ~0.5 m (Figures 4–8). By comparing water levels on the marsh with plant height (Table 1), we deduce that WLC occurs in the part of the water column occupied by plants. Therefore, the transport of water did not occur through sheet flow during the selected temporal windows and tidal conditions.

5.3. Temporal Variability in Hydrodynamic Conditions

Water movement in wetlands depends on two major drivers, namely tides and wind. While the former has a cyclical character, the latter is episodic in nature and can even vary from year to year (e.g., Donatelli et al., 2022a; Donatelli et al., 2022b). WLC on marshes may differ due to tidal variations (e.g., spring-neap modulation), fresh-water discharge, wind speed and direction, and duration of wind events (e.g., Gerkema & Duran-Matute, 2017; Valentine & Mariotti, 2019). Obviously, this type of UAVSAR flight campaign with repeated imaging within a single flight cannot reveal changes across the range of time scales. This remote sensing technique can only provide multiple images of WLC beneath the vegetation canopy within a short temporal window (i.e., it offers hydrodynamic information at an hourly time scale).

As documented by previous studies, meteorological events have a paramount effect on water levels in Terrebonne Bay (e.g., Reed, 1989), implying that WLC on marsh platforms can strongly deviate from its long-term statistics (i.e., long-term mean and/or median). In other words, the WLC measured by the two UAVSAR campaigns might not be representative of the typical hydrodynamic conditions experienced by salt marshes during ebb tide. To explore the temporal variability of such changes in water level at short- and long-time scales, a combination of UAVSAR images and numerical modeling is needed (e.g., Zhang, Jones, et al., 2022; Zhang, Wright, et al., 2022). This task is not trivial, especially if we want to investigate marsh hydrodynamics at a very high spatial resolution, which this study indicates is important, and at the same time employ numerical simulations spanning several years (e.g., Donatelli et al., 2022b). In fact, a grid size of ~1 m would dramatically increase the simulation time and consequently reduce the performance of the model, while a model with a larger resolution (e.g., 10 m) would not be able to consider the effect of levees and small channel on WLC within vegetated areas.

5.4. Implications for Coastal Vulnerability Predictions

This new generation of remotely sensed data can also be used to achieve precise estimation of fluxes of water and its constituents in coastal environments, which is essential to evaluate the impact of climate change on wetlands. A robust quantification of such fluxes allows us to predict which parts of a salt-marsh system will erode and which parts will grow; this information can be employed, for instance, to design effective interventions along the shoreline, and forecast the location and timing of new land creation through sediment accumulation (e.g., Tas et al., 2022; Winterwerp et al., 2020). Additionally, UAVSAR observations may be applied to improve the accuracy of numerical models to simulate hydrodynamics within vegetated areas, which is fundamental to quantify the impact of future extreme events on coastal communities (e.g., Aretxabaleta et al., 2019; Temmerman et al., 2022). A better understanding of how water levels are impacted by vegetation is important to limit the economic impact of coastal hazards and increase the capability of communities and coastal economies to recover (e.g., Goreau & Hilbertz, 2005).

6. Conclusions

The main conclusions of this paper can be summarized as follows:

1. UAVSAR can measure changes in water level across salt marshes at an unprecedented spatial resolution. These data prove reliable in capturing the effect of small geomorphic features (width smaller than 10 m) on WLC within these vegetated environments.
2. We utilized UAVSAR data to investigate drainage patterns over three salt marshes in Terrebonne Bay, USA. Our study shows that these marshes exhibit substantial variability in WLC during falling tides.

3. Small tidal channels and levees affect WLC on marsh surfaces. More specifically, these geomorphic elements affect water transport within the adjacent vegetated areas and, as a consequence, influence WLC. This finding explains why portions of a marsh characterized by the same elevation can drain water differently.
4. The presence of small channels in marshes can be easily detected via UAVSAR by mapping the spatial distribution of WLC.
5. Vegetation has a minimal effect on water retention in the selected marshes. Our results suggest that in highly channelized marshes, spatial and seasonal changes in AGB do not have a substantial influence on WLC. This result implies that water transport during ebb tides occurs mainly through channels, and as such, vegetation has a small influence in retaining water on platforms.

Data Availability Statement

The data of aboveground biomass (AGB) from AVIRIS-NG can be accessed through the ORNL DAAC, which is open for public access and download (Jensen et al., 2021): <https://doi.org/10.3334/ORNLDAAC/1822>. The data of water-level change (WLC) from UAVSAR can be accessed and downloaded through the ORNL DAAC (Jones et al., 2022): <https://doi.org/10.3334/ORNLDAAC/2058>. The digital elevation model (DEM) can be accessed and downloaded through the ORNL DAAC (Christensen et al., 2023): <https://doi.org/10.3334/ORNLDAAC/2181>.

References

- Alsdorf, D. E., Rodriguez, E., & Lettenmaier, D. P. (2007). Measuring surface water from space. *Reviews of Geophysics*, 45(2), RG2002. <https://doi.org/10.1029/2006rg000197>
- Aretxabaleta, A. L., Ganju, N. K., Defne, Z., & Signell, R. P. (2019). Spatial distribution of water level impacting back-barrier bays. *Natural Hazards and Earth System Sciences*, 19(8), 1823–1838. <https://doi.org/10.5194/nhess-19-1823-2019>
- Ayoub, F., Jones, C. E., Lamb, M. P., Holt, B., Shaw, J. B., Mohrig, D., & Wagner, W. (2018). Inferring surface currents within submerged, vegetated deltaic islands and wetlands from multi-pass airborne SAR. *Remote Sensing of Environment*, 212, 148–160. <https://doi.org/10.1016/j.rse.2018.04.035>
- Beudin, A., Kalra, T. S., Ganju, N. K., & Warner, J. C. (2016). Development of a coupled wave-flow vegetation interaction model. *Computers & Geosciences*, 100, 76–86. <https://doi.org/10.1016/j.cageo.2016.12.010>
- Beudin, A., Kalra, T. S., Ganju, N. K., & Warner, J. C. (2017). Development of a coupled wave-flow vegetation interaction model. *Computers & Geosciences*, 100, 76–86. <https://doi.org/10.1016/j.cageo.2016.12.010>
- Blanton, J. O., Garrett, A. J., Bollinger, J. S., Hayes, D. W., Koffman, L. D., Amft, J., & Morre, T. (2010). Transport and retention of a conservative tracer in an isolated creek-marsh system. *Estuarine, Coastal and Shelf Science*, 87(2), 333–345. <https://doi.org/10.1016/j.ecss.2010.01.010>
- Carniello, L., D'Alpaos, A., & Defina, A. (2011). Modeling wind waves and tidal flows in shallow micro-tidal basins. *Estuarine, Coastal and Shelf Science*, 92(2), 263–276. <https://doi.org/10.1016/j.ecss.2011.01.001>
- Castañeda-Moya, E., & Solohin, E. (2021). *Delta-X: Aboveground vegetation structure for herbaceous wetlands across MRD, LA, USA*. ORNL DAAC. <https://doi.org/10.3334/ORNLDAAC/1997>
- Castañeda-Moya, E., & Solohin, E. (2022). *Delta-X: Belowground biomass and necromass across wetlands in the MRD, LA, USA, 2021*. ORNL DAAC. <https://doi.org/10.3334/ORNLDAAC/1999>
- Cathcart, C., Shaw, J., & Amos, M. (2020). Validation of streaklines as recorders of synoptic flow direction in a deltaic setting. *Remote Sensing*, 12(1), 148. <https://doi.org/10.3390/rs12010148>
- Christensen, A. L., Denbina, M. W., & Simard, M. (2023). *Delta-X: Digital elevation model, MRD, LA, USA, 2021* [Dataset]. ORNL DAAC. <https://doi.org/10.3334/ORNLDAAC/2181>
- Cooper, H. M., Zhang, C., Davis, S. E., & Troxler, T. G. (2019). Object-based correction of LiDAR DEMs using RTK-GPS data and machine learning modeling in the coastal Everglades. *Environmental Modelling & Software*, 112, 179–191. <https://doi.org/10.1016/j.envsoft.2018.11.003>
- Cortese, L., Donatelli, C., Zhang, X., Nghiem, J. A., Simard, M., Jones, C. E., et al. (2023). Coupling numerical models of deltaic wetlands with AirSWOT, UAVSAR, and AVIRIS-NG remote sensing data [Dataset]. *Biogeosciences Discussions*. [preprint] in review. <https://doi.org/10.5194/bg-2023-108>
- Cortese, L., & Fagherazzi, S. (2022). Fetch and distance from the bay control accretion and erosion patterns in Terrebonne marshes (Louisiana, USA). *Earth Surface Processes and Landforms*, 47(6), 1455–1465. <https://doi.org/10.1002/esp.5327>
- Costanza, R., de Groot, R., Braat, L., Kubiszewski, I., Fioramonti, L., Sutton, P., et al. (2017). Twenty years of ecosystem services: How far have we come and how far do we still need to go? *Ecosystem Services*, 28, 1–16. <https://doi.org/10.1016/j.ecoser.2017.09.008>
- Costanza, R., de Groot, R., Sutton, P., van der Ploeg, S., Anderson, S. J., Kubiszewski, I., et al. (2014). Changes in the global value of ecosystem services. *Global Environmental Change*, 26, 152–158. <https://doi.org/10.1016/j.gloenvcha.2014.04.002>
- Daboor, M., & Brisco, B. (2018). Wetland monitoring using synthetic aperture radar imagery. In D. Gökçe (Ed.), *Wetlands management-assessing risk and sustainable solutions* (pp. 61–84). IntechOpen. <https://doi.org/10.5772/32009>
- Donatelli, C., Duran-Matute, M., Gräwe, U., & Gerkema, T. (2022a). Residual circulation and freshwater retention within an event-driven system of intertidal basins. *Journal of Sea Research*, 186, 102242. <https://doi.org/10.1016/j.seares.2022.102242>
- Donatelli, C., Duran-Matute, M., Gräwe, U., & Gerkema, T. (2022b). Statistical detection of spatio-temporal patterns in the salinity field within an inter-tidal basin. *Estuaries and Coasts*, 45(8), 2345–2361. <https://doi.org/10.1007/s12237-022-01089-3>
- Donatelli, C., Ganju, N. K., Kalra, T., Fagherazzi, S., & Leonardi, N. (2019). Changes in hydrodynamics and wave energy as a result of seagrass decline along the shoreline of a microtidal back-barrier estuary. *Advances in Water Resources*, 128, 183–192. <https://doi.org/10.1016/j.advwatres.2019.04.017>
- Donatelli, C., Passalacqua, P., Wright, K., Salter, G., Lamb, M. P., Jensen, D., & Fagherazzi, S. (2023). Quantifying flow velocities in river deltas via remotely sensed suspended sediment concentration. *Geophysical Research Letters*, 50(4), e2022GL101392. <https://doi.org/10.1029/2022GL101392>

- Fagherazzi, S., Hannon, M., & D'Odorico, P. (2008). Geomorphic structure of tidal hydrodynamics in salt marsh creeks. *Water Resources Research*, 44(2), W02419. <https://doi.org/10.1029/2007WR006289>
- Fagherazzi, S., Kirwan, M. L., Mudd, S. M., Guntenspergen, G. R., Temmerman, S., D'Alpaos, A., et al. (2012). Numerical models of salt marsh evolution: Ecological, geomorphic, and climatic factors. *Reviews of Geophysics*, 50(1), RG1002. <https://doi.org/10.1029/2011RG000359>
- Fore, A. G., Chapman, B. D., Hawkins, B. P., Hensley, S., Jones, C. E., Michel, T. R., & Muellerschoen, R. J. (2015). UAVSAR polarimetric calibration. *IEEE Transactions on Geoscience and Remote Sensing*, 53(6), 3481–3491. <https://doi.org/10.1109/TGRS.2014.2377637>
- French, J. R., & Spencer, T. (1993). Dynamics of sedimentation in a tide-dominated back-barrier salt marsh, Norfolk, UK. *Marine Geology*, 110(3–4), 315–331. [https://doi.org/10.1016/0025-3227\(93\)90091-9](https://doi.org/10.1016/0025-3227(93)90091-9)
- Ganju, N. K., Defne, Z., Kirwan, M. L., Fagherazzi, S., D'Alpaos, A., & Carniello, L. (2017). Spatially integrative metrics reveal hidden vulnerability of microtidal salt marshes. *Nature Communications*, 8(1), 14156. <https://doi.org/10.1038/ncomms14156>
- Ganju, N. K., Nidzicko, N. J., & Kirwan, M. L. (2013). Inferring tidal wetland stability from channel sediment fluxes: Observations and a conceptual model. *Journal of Geophysical Research: Earth Surface*, 118(4), 2045–2058. <https://doi.org/10.1002/jgrf.20143>
- Garcia-Pineda, O., MacDonald, I., Hu, C., Svejksky, J., Hess, M., Dukhovskoy, D., & Morey, S. (2013). Detection of floating oil anomalies from the Deepwater Horizon oil spill with synthetic aperture radar. *Oceanography*, 26(2), 124–137. <https://doi.org/10.5670/oceanog.2013.38>
- Gerkema, T. (2019). *An introduction to tides*. (p. 214). Cambridge University Press. <https://doi.org/10.1017/9781316998793>
- Gerkema, T., & Duran-Matute, M. (2017). Interannual variability of mean sea level and its sensitivity to wind climate in an inter-tidal basin. *Earth System Dynamics*, 8(4), 1223–1235. <https://doi.org/10.5194/esd-8-1223-2017>
- Goreau, T., & Hilbertz, W. (2005). Marine ecosystem restoration: Costs and benefits for coral reefs. *World Resource Review*, 17(3), 375–409.
- Greenberg, E., Thompson, D. R., Jensen, D., Townsend, P. A., Queally, N., Chlus, A., et al. (2022). An improved scheme for correcting remote spectral surface reflectance simultaneously for terrestrial BRDF and water-surface sunglint in coastal environments. *Journal of Geophysical Research: Biogeosciences*, 127(3), e2021JG006712. <https://doi.org/10.1029/2021JG006712>
- Hanssen, R. (2001). *Radar interferometry*. Kluwer Academic Publishers.
- Hensley, S., Wheeler, K., Sadowy, G., Jones, C., Shaffer, S., Zebker, H., & Smith, R. (2008). The UAVSAR instrument: Description and first results. In *2008 IEEE radar conference* (pp. 1–6). IEEE. <https://doi.org/10.1109/RADAR.2008.4720722>
- Hetland, R. D., & DiMarco, S. F. (2008). The effects of bottom oxygen demand in controlling the structure of hypoxia on the Texas–Louisiana continental shelf. *Journal of Marine Systems*, 70(1–2), 49–62. <https://doi.org/10.1016/j.jmarsys.2007.03.002>
- Horstman, E. M., Dohmen-Janssen, C. M., Bouma, T. J., & Hulscher, S. J. M. H. (2015). Tidal-scale flow routing and sedimentation in mangrove forests: Combining field data and numerical modelling. *Geomorphology*, 228, 244–262. <https://doi.org/10.1016/j.geomorph.2014.08.011>
- Jensen, D., Simard, M., Cavanaugh, K., Sheng, Y., Fichot, C. G., Pavelsky, T., & Twilley, R. (2019). Improving the transferability of suspended solid estimation in wetland and deltaic waters with an empirical hyperspectral approach. *Remote Sensing*, 11(13), 1629. <https://doi.org/10.3390/RS11131629>
- Jensen, D., Thompson, D., Simard, M., Solohin, E., & Castañeda-Moya, E. (2023). Imaging spectroscopy-based estimation of aboveground biomass in Louisiana's coastal wetlands: Towards consistent spectroscopic retrievals across atmospheric states. In *In review at remote sensing of environment*.
- Jensen, D. J., Castañeda-Moya, E., Solohin, E., Rovai, A., Thompson, D. R., & Simard, M. (2023). Delta-X: AVIRIS-NG L3 derived aboveground biomass, MRD, Louisiana, USA, 2021, V2 [Dataset]. ORNL DAAC. <https://doi.org/10.3334/ORNLDAAC/2138>
- Jensen, D. J., Cavanaugh, K. C., Thompson, D. R., Fagherazzi, S., Cortese, L., & Simard, M. (2022). Leveraging the historical Landsat catalog for a remote sensing model of wetland accretion in coastal Louisiana. *Journal of Geophysical Research: Biogeosciences*, 127(6), e2022JG006794. <https://doi.org/10.1029/2022JG006794>
- Jensen, D. J., Simard, M., Fichot, C. G., & Pavelsky, T. M. (2021). *Pre-delta-X: AVIRIS-derived total suspended solids maps for MRD*. ORNL DAAC. <https://doi.org/10.3334/ORNLDAAC/1822>
- Jones, C., Oliver-Cabrera, T., Varugu, B., Simard, M., & Lou, Y. (2022). Delta-X: UAVSAR L3 water level changes, MRD, Louisiana, 2021 [Dataset]. ORNL DAAC. <https://doi.org/10.3334/ORNLDAAC/2058>
- Leonardi, N., Carnacina, I., Donatelli, C., Ganju, N. K., Plater, A. J., Schuerch, M., & Temmerman, S. (2018). Dynamic interactions between coastal storms and salt marshes. *A review: Geomorphology*, 301, 92–107. <https://doi.org/10.1016/j.geomorph.2017.11.001>
- Liao, W., & Jiang, W. (2020). Evaluation of the spatiotemporal variations in the eco environmental quality in China based on the remote sensing ecological index. *Remote Sensing*, 12(15), 2462. <https://doi.org/10.3390/rs12152462>
- Lu, Z., & Kwoun, O. I. (2008). Radarsat-1 and ERS InSAR analysis over southeastern coastal Louisiana: Implications for mapping water-level changes beneath swamp forests. *IEEE Transactions on Geoscience and Remote Sensing*, 46(8), 2167–2184. <https://doi.org/10.1109/tgrs.2008.917271>
- Marani, M., D'Alpaos, A., Lanzoni, S., Carniello, L., & Rinaldo, A. (2007). Biologically-controlled multiple equilibria of tidal landforms and the fate of the Venice lagoon. *Geophysical Research Letters*, 34(11), L11402. <https://doi.org/10.1029/2007GL030178>
- Marani, M., D'Alpaos, A., Lanzoni, S., Carniello, L., & Rinaldo, A. (2010). The importance of being coupled: Stable states and catastrophic shifts in tidal biomorphodynamics. *Journal of Geophysical Research*, 115(F4), F04004. <https://doi.org/10.1029/2009JF001600>
- Marani, M., D'Alpaos, A., Lanzoni, S., & Santalucia, M. (2011). Understanding and predicting wave erosion of marsh edges. *Geophysical Research Letters*, 38(21), L21401. <https://doi.org/10.1029/2011GL048995>
- Mariotti, G. (2016). Revisiting salt marsh resilience to sea level rise: Are ponds responsible for permanent land loss? *Journal of Geophysical Research: Earth Surface*, 121(7), 1391–1407. <https://doi.org/10.1002/2016JF003900>
- Mariotti, G., & Fagherazzi, S. (2010). A numerical model for the coupled long-term evolution of salt marshes and tidal flats. *Journal of Geophysical Research*, 115(F1), F01004. <https://doi.org/10.1029/2009JF001326>
- Mazda, Y., Magi, M., Kogo, M., & Hong, P. N. (1997). Mangroves as a coastal protection from waves in the tong king delta, Vietnam. *Mangroves and Salt Marshes*, 1(2), 127–135. <https://doi.org/10.1023/a:1009928003700>
- Medeiros, S., Hagen, S., Weishampel, J., & Angelo, J. (2015). Adjusting lidar-derived digital terrain models in coastal marshes based on estimated aboveground biomass density. *Remote Sensing*, 7(4), 3507–3525. <https://doi.org/10.3390/rs70403507>
- Montgomery, J. M., Bryan, K. R., Horstman, E. M., & Mullarney, J. C. (2018). Attenuation of tides and surges by mangroves: Contrasting case studies from New Zealand. *Water*, 10(9), 1119. <https://doi.org/10.3390/w10091119>
- Mudd, S. M., D'Alpaos, A., & Morris, J. T. (2010). How does vegetation affect sedimentation on tidal marshes? Investigating particle capture and hydrodynamic controls on biologically mediated sedimentation. *Journal of Geophysical Research*, 115(F3), F03029. <https://doi.org/10.1029/2009JF001326>
- Nepf, H. M. (2012). Flow and transport in regions with aquatic vegetation. *Annual Review of Fluid Mechanics*, 44(1), 123–142. <https://doi.org/10.1146/annurev-fluid-120710-101048>

- Oliver-Cabrera, T., Jones, C. E., Yunjun, Z., & Simard, M. (2021). InSAR phase unwrapping error correction for rapid repeat measurements of water level change in wetlands. *IEEE Transactions on Geoscience and Remote Sensing*, *60*, 1–15. <https://doi.org/10.1109/TGRS.2021.3108751>
- Oliver-Cabrera, T., & Wdowski, S. (2016). InSAR-based mapping of tidal inundation extent and amplitude in Louisiana coastal wetlands. *Remote Sensing*, *8*(5), 393. <https://doi.org/10.3390/rs8050393>
- Orton, P. M., Sanderson, E. W., Talke, S. A., Giampieri, M., & MacManus, K. (2020). Storm tide amplification and habitat changes due to urbanization of a lagoonal estuary. *Natural Hazards and Earth System Sciences*, *20*(9), 2415–2432. <https://doi.org/10.5194/nhess-20-2415-2020>
- Pannoza, N., Leonardi, N., Carnacina, I., & Smedley, R. (2021). Salt marsh resilience to sea-level rise and increased storm intensity. *Geomorphology*, *389*, 107825. <https://doi.org/10.1016/j.geomorph.2021.107825>
- Pelckmans, I., Belliard, J. P., Dominguez-Granda, L. E., Slobbe, C., Temmerman, S., & Gourgue, O. (2023). Mangrove ecosystem properties regulate high water levels in a river delta [Dataset]. EGU sphere. [preprint]. <https://doi.org/10.5194/egusphere-2023-428>
- Peteet, D. M., Nichols, J., Kenna, T., Chang, C., Browne, J., Reza, M., et al. (2018). Sediment starvation destroys New York City marshes' resistance to sea level rise. *Proceedings of the National Academy of Sciences of the United States of America*, *115*(41), 10281–10286. <https://doi.org/10.1073/pnas.1715392115>
- Reed, D. J. (1989). Patterns of sediment deposition in subsiding coastal salt marshes, Terrebonne bay, Louisiana: The role of winter storms. *Estuaries and Coasts*, *12*(4), 222–227. <https://doi.org/10.2307/1351901>
- Rogers, J. N., Parrish, C. E., Ward, L. G., & Burdick, D. M. (2018). Improving salt marsh digital elevation model accuracy with full-waveform lidar and nonparametric predictive modeling. *Estuarine, Coastal and Shelf Science*, *202*, 193–211. <https://doi.org/10.1016/j.ecss.2017.11.034>
- Rosen, P. A., Hensley, S., Joughin, I. R., Li, F. K., Madsen, S. N., Rodriguez, E., & Goldstein, R. M. (2000). Synthetic aperture radar interferometry. In *Proceeding of the IEEE* (Vol. 88, pp. 333–382).
- Schuerch, M., Spencer, T., Temmerman, S., Kirwan, M. L., Wolff, C., Lincke, D., et al. (2018). Future response of global coastal wetlands to sea-level rise. *Nature*, *561*(7722), 231–234. <https://doi.org/10.1038/s41586-018-0476-5>
- Sullivan, J. C., Torres, R., & Garrett, A. (2019). Intertidal creeks and overmarsh circulation in a small salt marsh basin. *Journal of Geophysical Research: Earth Surface*, *124*(2), 447–463. <https://doi.org/10.1029/2018jfo04861>
- Tas, S. A. J., van Maren, D. S., & Reniers, A. J. H. M. (2022). Chenier formation through wave winnowing and tides. *Journal of Geophysical Research: Earth Surface*, *127*, e2022JF006792. <https://doi.org/10.1029/2022JF006792>
- Temmerman, S., Bouma, T. J., Govers, G., & Lauwaet, D. (2005). Flow paths of water and sediment in a tidal marsh: Relations with marsh developmental stage and tidal inundation height. *Estuaries*, *28*(3), 338–352. <https://doi.org/10.1007/BF02693917>
- Temmerman, S., Bouma, T. J., Van de Koppel, J., Van der Wal, D., De Vries, M. B., & Herman, P. M. J. (2007). Vegetation causes channel erosion in a tidal landscape. *Geology*, *35*(7), 631–634. <https://doi.org/10.1130/G23502A.1>
- Temmerman, S., Horstman, E. M., Krauss, K. W., Mullarney, J. C., Pelckmans, I., & Schoutens, K. (2022). Marshes and mangroves as nature-based coastal storm buffers. *Annual Review of Marine Science*, *15*(1), 95–118. <https://doi.org/10.1146/annurev-marine-040422-092951>
- Temmerman, S., Meire, P., Bouma, T. J., Herman, P. M. J., Ysebaert, T., & De Vriend, H. J. (2013). Ecosystem-based coastal defence in the face of global change. *Nature*, *504*(7478), 79–83. <https://doi.org/10.1038/nature12859>
- Thompson, D. R., Cawse-Nicholson, K., Erickson, Z., Fichot, C. G., Frankenberg, C., Gao, B.-C., et al. (2019). A unified approach to estimate land and water reflectances with uncertainties for coastal imaging spectroscopy. *Remote Sensing of Environment*, *231*, 111198. <https://doi.org/10.1016/j.rse.2019.05.017>
- Thompson, D. R., Jensen, D. J., Chapman, J. W., Simard, M., & Greenberg, E. (2022). *Delta-X: AVIRIS-NG BRDF-adjusted surface reflectance, MRD, LA, 2021*. ORNL DAAC. <https://doi.org/10.3334/ORNLDAAAC/2025>
- Valentine, K., & Mariotti, G. (2019). Wind-driven water level fluctuations drive marsh edge erosion variability in microtidal coastal bays. *Continental Shelf Research*, *176*, 76–89. <https://doi.org/10.1016/j.csr.2019.03.002>
- Wiberg, P. L., Fagherazzi, S., & Kirwan, M. L. (2020). Improving predictions of salt marsh evolution through better integration of data and models. *Annual Review of Marine Science*, *12*(1), 389–413. <https://doi.org/10.1146/annurev-marine-010419-010610>
- Winterwerp, J. C., Albers, T., Anthony, E. J., Friess, D. A., Mancheño, A. G., Moseley, K., et al. (2020). Managing erosion of mangrove-mud coasts with permeable dams—lessons learned. *Ecological Engineering*, *158*, 106078. <https://doi.org/10.1016/j.ecoleng.2020.106078>
- Wright, K., Passalacqua, P., Simard, M., & Jones, C. E. (2022). Integrating connectivity into hydrodynamic models: An automated open-source method to refine an unstructured mesh using remote sensing. *Journal of Advances in Modeling Earth Systems*, *14*(8), e2022MS003025. <https://doi.org/10.1029/2022ms003025>
- Wu, Y., Thorne, E. T., Sharp, R. E., & Cosgrove, D. J. (2001). Modification of expansin transcript levels in the maize primary root at low water potentials. *Plant Physiology*, *126*(4), 1471–1479. <https://doi.org/10.1104/pp.126.4.1471>
- Xu, Y., Kalra, T. S., Ganju, N. K., & Fagherazzi, S. (2022). Modeling the dynamics of salt marsh development in coastal land reclamation. *Geophysical Research Letters*, *49*(6), e2021GL095559. <https://doi.org/10.1029/2021GL095559>
- Zhang, X., Jones, C. E., Oliver-Cabrera, T., Simard, M., & Fagherazzi, S. (2022). Using rapid repeat SAR interferometry to improve hydrodynamic models of food propagation in coastal wetlands. *Advances in Water Resources*, *159*, 104088. Article ID 104088. <https://doi.org/10.1016/j.advwatres.2021.104088>
- Zhang, X., Wright, K., Passalacqua, P., Simard, M., & Fagherazzi, S. (2022). Improving channel hydrological connectivity in coastal hydrodynamic models with remotely sensed channel networks. *Journal of Geophysical Research: Earth Surface*, *127*(3), e2021JF006294. <https://doi.org/10.1029/2021jf006294>